Research Article

Vol. 13, No. 6 / June 2026 / Optica 1137

OPTICA

# Generalized photon-bunching bounds in linear and non-linear quantum optical dynamics

Tommaso Francalanci,[1] Giovanni Rodari,[1] Eugenio Caruccio,[1] Francesco Hoch,[1] Gonzalo Carvacho,[1] Taira Giordani,[1] Nicolò Spagnolo,[1] Riccardo Albiero,[2] Niki Di Giano,[2,3] Giacomo Corrielli,[2] Francesco Ceccarelli,[2] Roberto Osellame,[2] Ulysse Chabaud,[4] and Fabio Sciarrino[1,*]

[1] Dipartimento di Fisica, Sapienza Università di Roma, Piazzale Aldo Moro 5, Roma 00185, Italy
[2] Istituto di Fotonica e Nanotecnologie, Consiglio Nazionale delle Ricerche (IFN-CNR), Piazza Leonardo da Vinci 32, Milano 20133, Italy
[3] Dipartimento di Fisica, Politecnico di Milano, Piazza Leonardo da Vinci 32, Milano 20133, Italy
[4] DIENS, École Normale Supérieure, PSL University, CNRS, INRIA, 45 rue d'Ulm, Paris 75005, France
*fabio.sciarrino@uniroma1.it

Received 18 September 2025; revised 13 April 2026; accepted 13 April 2026; published 12 June 2026

**To assess the capabilities of photonic quantum systems, it is essential to develop analytical and experimental methods for probing the underlying optical dynamics. Here, we investigate fundamental constraints arising when multi-photon states evolve through a quantum linear optical network, showing how such limitations can be overcome when introducing measurement-induced nonlinearities. Specifically, we analyze bounds related to photon-bunching behavior at the output of a linear interferometer and test them via a hybrid photonic platform realizing experiments with up to four photons. When the analysis is extended to a nonlinear regime, such bounds can be violated. We experimentally validate such behavior by employing an optical architecture featuring measurement-induced nonlinearity, thus introducing dynamics that go beyond standard linear optics. Our results highlight how the constraints implied by the linear optical formalism can be used as tools to test and characterize photonic models going beyond quantum linear optical dynamics.** 

https://doi.org/10.1364/OPTICA.579537

## 1. INTRODUCTION

In recent years, quantum linear optical systems have gained significant attention as a promising platform for photonic-based quantum information processing. Within this framework, boson sampling has emerged as a paradigmatic model to demonstrate quantum computational advantage, exploiting multi-photon interference to generate output distributions believed to be classically intractable [1–4]. Several large-scale implementations have been reported [5–12], highlighting the need for robust techniques to characterize the output distributions of linear optical dynamics. Most previous work has focused on validating these dynamics against alternative classical or noisy distributions [13–20]. In contrast to such validation-focused approaches, here we investigate the quantum dynamics imposed by a linear optical transformation and the nature of bosonic interference. Can one identify measurable bounds, which are intrinsically related to linear dynamics? On the one hand, this can offer new insights on the capabilities of linear optical transformations for quantum information processing purposes. On the other hand, such analysis can become relevant in the broader context of enhanced photonic schemes [21–23], where measurement-induced nonlinearities are introduced to go beyond linear dynamics.

The impossibility of generating arbitrary output states from the linear optical evolution of a fixed input state is well established [24]. However, the precise structure of the reachable output space remains largely unexplored. Several efforts have been made to characterize this space. One approach focuses on identifying the set of Fock-space unitary transformations accessible via linear optics [25,26]. Another line of work is based on algebraic invariants [27–30], which remain conserved under linear optical evolution. These approaches already provide valuable information about the structure of linear optical dynamics, typically relying on the estimation of specific observables or invariant quantities constructed from photon-counting data.

Here, we take a complementary approach by investigating what can be learned directly from output state populations, namely the photon-counting statistics. In contrast to approaches based on expectation values of observables, the method proposed here directly probes features of the output photon-number distribution, and is therefore naturally sensitive to multi-photon interference effects and particle indistinguishability. We focus in particular on full-bunching probabilities, which correspond to the events where all photons are detected in the same output mode. These probabilities have been primarily studied in the context of validating boson sampling against classical or noisy alternatives [14,31–33], where

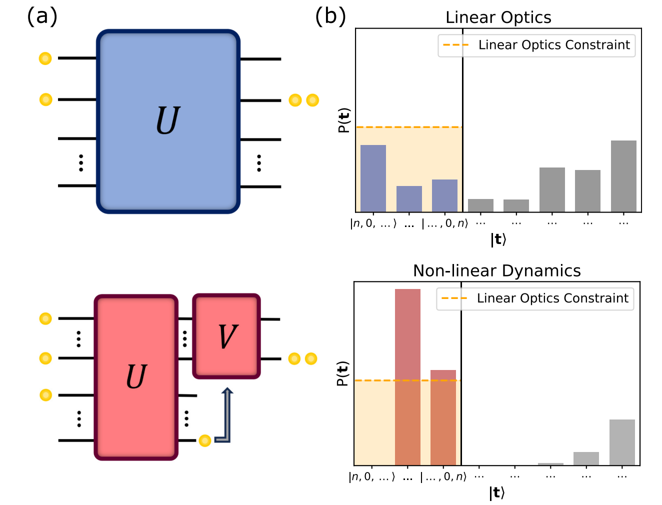


**Fig. 1.** (a) Conceptual schemes illustrating two photonic architectures: on the top is a model implementing a purely linear optical evolution; on the bottom is a model where effective non-linear dynamics are introduced by measuring part of the photons in auxiliary modes. (b) Illustrative output distributions corresponding to the two schemes, with a focus on full-bunching events (colored bars). In the linear optics case (blue), the bunching probabilities lie below the theoretical bound (dashed line), while in the non-linear scenario (red), some bunching events exceed it, highlighting a violation of linear-optical constraints.

photon bunching is known to be enhanced by indistinguishability. Moreover, bunching probabilities have also been studied in the context of multi-photon interference effects with partially distinguishable resources [34,35].

Overall, our goal is not to establish a full validation or certification protocol, but rather to introduce a simple and experimentally accessible witness based on necessary conditions that any evolution governed by linear optics must satisfy. We derive theoretical constraints on full-bunching probabilities and experimentally verify them using a demultiplexed single-photon source, a fully reconfigurable photonic integrated circuit, and a pseudo-photon-number-resolving detection scheme based on threshold detectors. Moreover, we extend our analysis to a class of experiments that go beyond the linear optics regime. In these setups, analogous to the ones of [21,22], part of the photons are measured in auxiliary modes, and post-selection is used to emulate measurement-induced nonlinearity. We show that, unlike standard linear optical evolution, such non-linear processes can produce output distributions that violate the full-bunching constraints, revealing their ability to access regions of the output space that are otherwise forbidden, as illustrated in the conceptual picture of Fig. 1.

## 2. CONSTRAINTS ON FULL-BUNCHING PROBABILITIES

In the following, we introduce several criteria to determine if a given output state can be obtained with a standard linear optical boson sampling setup. This approach is related to the output probabilities of full-bunching events, corresponding to all the photons emerging in the same mode from the optical evolution. In particular, we consider a boson sampling experiment with $n$ photons going through $m$ modes with $m \geq n$. A generic input state in this configuration is given by $|\boldsymbol{s}\rangle = |s_1, \ldots, s_m\rangle$, where $\{s_i\}$ is a set of integers indicating the number of photons in each mode and $\sum_{i=1}^m s_i = n$. We then consider the linear optical evolution of this input state, which can be described by an arbitrary unitary transformation $U \in SU(m)$ of the modes. The probability of obtaining the output $|\boldsymbol{t}\rangle$ when the input is $|\boldsymbol{s}\rangle$ is given by [1]

$$P[\boldsymbol{s} \to \boldsymbol{t}] = \frac{|\mathrm{Per}(U_{\boldsymbol{s},\boldsymbol{t}})|^2}{s_1! \cdots s_m! t_1! \cdots t_m!}, \tag{1}$$

where $U_{\boldsymbol{s},\boldsymbol{t}}$ is the $n \times n$ matrix obtained by repeating $t_i$ times the $i$th row of $U$ and $s_j$ times the $j$th column of $U$, and $\mathrm{Per}(B)$ denotes the permanent of a matrix $B$ [36]. In the following, we derive constraints on full-bunching probabilities for specific input states as well as for general input states. To do so, we exploit the following relation valid for any unitary matrix $U \in SU(m)$:

$$\sum_{j=1}^{m} |U_{ij}|^2 = 1 \Rightarrow \sum_{j=1}^{n} |U_{ij}|^2 \leq 1, \tag{2}$$

where we notice that equality holds when $n = m$. Using Eqs. (1) and (2), we find polynomial relations for the full-bunching probabilities, giving rise to different kinds of constraints. In the following, we address some specific scenarios in more detail.

As a first example, we consider the full-bunching probabilities for the input $|\boldsymbol{s}\rangle = |1^{\otimes n} 0^{\otimes(n-m)}\rangle$ (type A). In the simplest case of two photons injected into two separate modes—akin to a generalized Hong–Ou–Mandel experiment [37,38]—it is well known that the probability of full-bunching cannot exceed 1/2 [24,38]. A more general result can be found in [39], where the following bound on the full-bunching probability is obtained

$$P_i^A := P\left[|1^{\otimes n} 0^{\otimes(m-n)}\rangle \to |0^{\otimes(i-1)}, n, 0^{\otimes(m-i)}\rangle\right] \leq \frac{n!}{n^n}. \tag{3}$$

Here, we recover this result with another approach, exploiting Eqs. (1, 2) directly. In particular, we notice that following Eq. (1) the probability of going from $|\boldsymbol{s}\rangle = |1^{\otimes n} 0^{\otimes(m-n)}\rangle$ to $|\boldsymbol{t}\rangle = |0^{\otimes(i-1)}, n, 0^{\otimes(m-i)}\rangle$ can be obtained as

$$P[\boldsymbol{s} \to \boldsymbol{t}] = \frac{1}{n!} \left| n! \prod_{j=1}^{n} U_{ij} \right|^2 = n! \prod_{j=1}^{n} |U_{ij}|^2, \tag{4}$$

where we exploited that all rows in the matrix $U_{\boldsymbol{s},\boldsymbol{t}}$ are equal. The AM-GM inequality states that the arithmetic mean (AM) of a list of non-negative real numbers is greater than or equal to its geometric mean (GM), i.e., $\sqrt[n]{\prod_{j=1}^n x_j} \leq \sum_{j=1}^n x_j/n$. Using the inequality with $x_j = |U_{ij}|^2$ we obtain

$$P[\boldsymbol{s} \to \boldsymbol{t}] = n! \prod_{j=1}^{n} |U_{ij}|^2 \leq n! \left( \frac{\sum_{j=1}^{n} |U_{ij}|^2}{n} \right)^n \leq \frac{n!}{n^n}, \tag{5}$$

where in the last step we exploited Eq. (2).

Notice that, as shown in [31], the probability in Eq. (4) is simply reduced by a factor $n!$ for distinguishable bosons. Thus, by replicating the above analysis, the following stricter bound is obtained for each full-bunching probability when considering distinguishable photons: $P_i^{A-\mathrm{dist}} \leq \frac{1}{n^n}$.

We now consider a different kind of input, specifically of the form $|\boldsymbol{s}\rangle = |n, 0, \ldots, 0\rangle$ (type B). The probability of obtaining the full-bunching output state $|\boldsymbol{t}\rangle = |0^{i-1}, n, 0^{m-i}\rangle$ in this case is given by

$$P[\boldsymbol{s} \to \boldsymbol{t}] = (|U_{i1}|^2)^n. \quad (6)$$

Here, we used Eq. (1) and exploited the fact that all elements in the matrix $U_{\boldsymbol{s},\boldsymbol{t}}$ are equal. We now define $P_{1i}^B$ as the probability of going from the full-bunching input state $|\boldsymbol{s}\rangle = |n, 0, \ldots, 0\rangle$ to the full-bunching output $|\boldsymbol{t}\rangle = |0^{i-1}, n, 0^{m-i}\rangle$:

$$P_{1i}^B := P\big[|n, 0^{\otimes(n-1)}\rangle \to |0^{\otimes(i-1)}, n, 0^{\otimes(m-i)}\rangle\big] = (|U_{i1}|^2)^n. \quad (7)$$

Using again Eq. (2) we obtain

$$\sum_{i=1}^{m} \sqrt[n]{P_{1i}^B} = 1. \quad (8)$$

Notice that, since the probability in Eq. (6) is identical for distinguishable photons, the constraint of Eq. (8) also applies in that case.

A more general bound can be derived for arbitrary Fock states of the form $|\boldsymbol{s}\rangle = |n_1, \ldots, n_m\rangle$, with $\sum_{j=1}^{m} n_j = n$. In this general case, the full-bunching probability admits an upper bound of the form:

$$P[\boldsymbol{s} \to \boldsymbol{t}] \le \frac{n!}{n^n} \prod_{j=1}^{m} \frac{n_j^{n_j}}{n_j!}. \quad (9)$$

A detailed derivation of Eq. (9) is provided in Supplement 1. This bound, which reduces to Eq. (3) for the previously discussed type A input, applies also to input states that do not fall into either the type A or type B classification. Notably, in the case of type B inputs, Eq. (9) reduces to the trivial condition $P[\boldsymbol{s} \to \boldsymbol{t}] \le 1$, so that Eq. (8) provides a stronger constraint for this specific case.

## 3. EXPERIMENTAL SETUP

To test the introduced constraints, we perform boson sampling experiments across different configurations with up to $n = 4$ photons and $m = 4$ modes. We also extend the same constraints to a non-linear regime where a subset of photons is measured in auxiliary modes, and the evolution of the remaining photons is conditioned on the measurement outcome. This strategy, inspired by the adaptive boson sampling (ABS) paradigm recently studied both theoretically and experimentally in [21,22], emulates measurement-induced nonlinearities via post-selection.

The experimental apparatus is based on a hybrid photonic platform developed specifically for the implementation of multi-photon experiments [22,29,40–43]. The single-photon source consists of a quantum dot [44–47], excited at a repetition rate of 79 MHz in the resonance fluorescence regime [45,48–51]. The emitted photons are time-to-spatial demultiplexed using an optical scheme based on an acousto-optic modulator. Temporal and polarization compensation is ensured by delay lines and polarization control plates, enabling the preparation of up to four indistinguishable photons.

These photons are injected into an eight-mode fully reconfigurable photonic integrated circuit, fabricated using femtosecond laser-writing techniques [52,53]. The circuit consists of a network of 28 Mach–Zehnder interferometers (MZIs) arranged in a rectangular mesh according to the scheme of [54]. Each MZI, equipped with thermo-optically tunable phase shifters [55–58], acts as a reconfigurable beam splitter. These elementary cells can be individually programmed, enabling the realization of arbitrary unitary transformations in $SU(m)$.

In the standard (linear optical) boson sampling regime, the interferometer is structured into two main sections, an input state preparation stage and a unitary transformation stage, as detailed in Supplement 1. The first stage is required to probabilistically prepare input states featuring more than one photon per mode, obtaining the generation of specific multi-photon Fock states by exploiting the Hong–Ou–Mandel effect [37,38]. The evolution stage then applies random unitary transformations using the architecture of [54].

In extended configurations that do involve intermediate measurements, a subset $r \le n$ of photons is detected in $k \le m$ auxiliary modes, akin to the aforementioned adaptive boson sampling (ABS) architecture [21,22], which is described in detail in Supplement 1. The measurement outcome $\boldsymbol{p} = (p_1, \ldots, p_k)$ determines a conditional linear unitary evolution of the modes $V(\boldsymbol{p})$ applied to the remaining $n' = n - r$ photons over the remaining $m' = m - k$ output modes. This procedure, although implemented via post-selection, effectively emulates a measurement-induced non-linear process. Thus, the implementation of the protocol via post-selection does indeed allow one to test the linearity bounds in effective non-linear dynamics.

Photon detection is performed using superconducting nanowire single-photon detectors. Since standard threshold detectors do not resolve photon numbers, we adopt a probabilistic pseudo-number-resolving scheme, as detailed in Supplement 1. Each output mode is split into four auxiliary modes using a cascade of 50:50 beam splitters, allowing us to reconstruct probabilities of output Fock states, including bunching events where at least one $n_i \ge 2$. The final statistics are obtained by collecting coincidences across auxiliary modes and correcting for the corresponding detection probabilities. To account for the probabilistic nature of both state preparation and detection, all data are post-selected on events where all $n$ (or $n'$) photons are detected in different auxiliary modes.

## 4. TESTING THE CONSTRAINTS IN LINEAR OPTICS

We now present the results of our experimental tests. To begin with, we consider the simplest configuration with $n = 2$ photons in $m = 2$ modes. In this case, we have only type A inputs such as $|1, 1\rangle$ or type B inputs such as $|2, 0\rangle$. We measure the full-bunching probabilities as obtained after evolving these inputs with 1000 different randomly drawn unitary transformations $U \in SU(2)$. In Fig. 2(a), we show scatter plots of the obtained probabilities for the two configurations, highlighting the constraint region for $|1, 1\rangle$ and the constraint curve for $|2, 0\rangle$, given by Eqs. (3) and (8), respectively. We see that both constraints are well satisfied, as detailed in the first row of Table 1. In the first plot, we also highlight the additional constraint $P(20) = P(02)$ (red dashed line), which holds for the input state $|1, 1\rangle$, as one can easily see from the representation in the Fock basis of the unitary evolution (see, e.g., [24]). Our experimental results also show evidence of this behavior, although small deviations are observed, likely due to slight imbalances in detector efficiency calibration.

To further test the constraints, we increase the number of photons and modes, considering configurations up to $n = 4$ and $m = 4$. In all the different configurations, we test the constraints for both types A and B scenarios. For $m = 4$ cases, we restrict our analysis to type A inputs due to the limited interferometer depth,

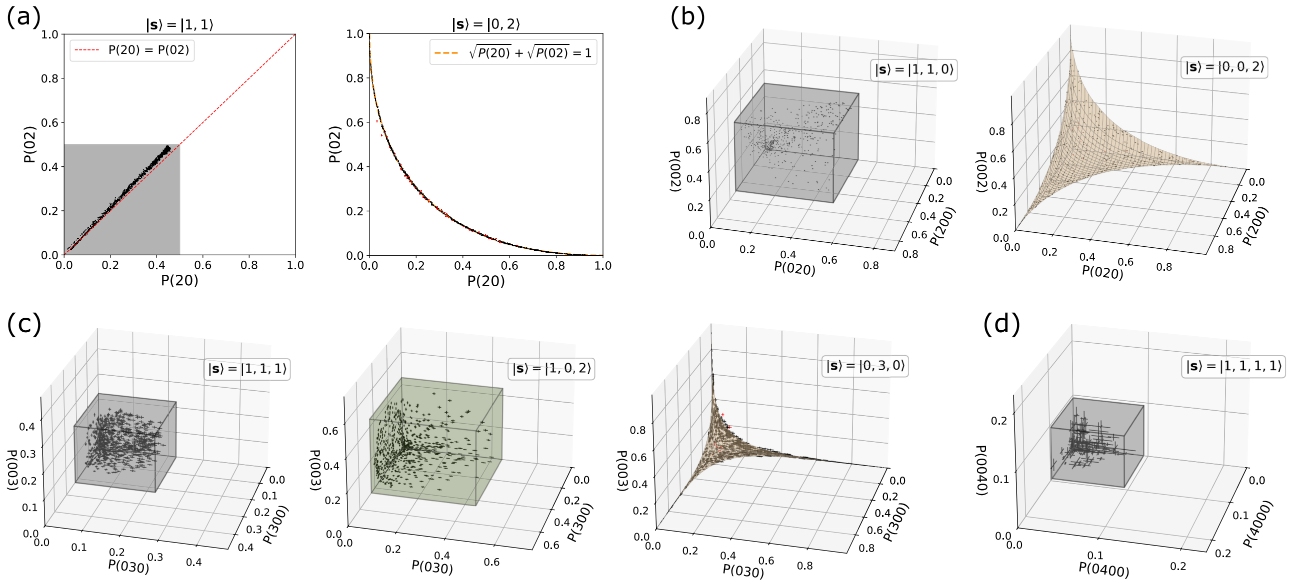


**Fig. 2.** (a) Scatter plot for the full-bunching probabilities as obtained with boson sampling experiments with randomly extracted $U \in SU(2)$ with input $|1, 1\rangle$ (type A) and $|0, 2\rangle$ (type B). We show with a gray square the constraint region for input $|1, 1\rangle$ and with an orange dashed line the constraint curve for input $|0, 2\rangle$. We also show with a red dashed line the additional constraint $P(20) = P(02)$ for the $|1, 1\rangle$ input. (b), (c) 3D scatter plot for the full-bunching probabilities as obtained with boson sampling experiments with randomly extracted $U \in SU(3)$ with (b) 2-photon inputs: $|1, 1, 0\rangle$ (type A) and $|2, 0, 0\rangle$ (type B), and (c) 3-photon inputs: $|1, 1, 1\rangle$ (type A), $|2, 1, 0\rangle$ and $|3, 0, 0\rangle$ (type B). In the plots, the constraints are represented by the colored surfaces (gray cube for type A inputs, green cube for $|2, 1, 0\rangle$ input, and orange surface for type B inputs). (d) 3D Scatter Plot for 3 of the 4 full-bunching probabilities as obtained with boson sampling experiments with randomly extracted $U \in SU(4)$ with 4-photon type A input $|1, 1, 1, 1\rangle$. In the plot, the type A constraint is represented by the gray cube. In all cases, error bars are given by uncertainties in photon counts due to Poisson statistics, and we highlight in red the points, which are not compatible within the error bars with the corresponding constraint.

**Table 1. Constraints on Full-Bunching Probabilities for Different Linear Optics Scenarios**[a]

| # Photons (n) | # Modes (m) | Input State $\lvert s\rangle$ | Constraint on Full-Bunching Probabilities | # States | States Satisfying the Constraints |
|---|---|---|---|---|---|
| 2 | 2 | $\lvert 1, 1\rangle$ (type A) | $P(20) \leq \frac{1}{2},\ P(02) \leq \frac{1}{2}$ | 1000 | 100% |
| | | $\lvert 0, 2\rangle$ (type B) | $\sqrt{P(20)} + \sqrt{P(02)} = 1$ | 1000 | 95.5% (99.7%) |
| 2 | 3 | $\lvert 1, 1, 0\rangle$ (type A) | $P(200),\ P(020),\ P(002) \leq \frac{1}{2}$ | 500 | 100% |
| | | $\lvert 0, 0, 2\rangle$ (type B) | $\sqrt{P(200)} + \sqrt{P(020)} + \sqrt{P(002)} = 1$ | 500 | 98.2% (100%) |
| 3 | 3 | $\lvert 1, 1, 1\rangle$ (type A) | $P(300),\ P(030),\ P(003) \leq \frac{2}{9}$ | 1000 | 100% |
| | | $\lvert 1, 0, 2\rangle$ | $P(300),\ P(030),\ P(003) \leq \frac{4}{9}$ | 1000 | 100% |
| | | $\lvert 0, 3, 0\rangle$ (type B) | $\sqrt[3]{P(300)} + \sqrt[3]{P(030)} + \sqrt[3]{P(003)} = 1$ | 1000 | 99% (99.8%) |
| 2 | 4 | $\lvert 0, 1, 1, 0\rangle$ (type A) | $P(2000),\ P(0200),\ P(0020),\ P(0002) \leq \frac{1}{2}$ | 400 | 100% |
| 3 | 4 | $\lvert 1, 1, 1, 0\rangle$ (type A) | $P(3000),\ P(0300),\ P(0030),\ P(0003) \leq \frac{2}{9}$ | 1250 | 100% |
| 4 | 4 | $\lvert 1, 1, 1, 1\rangle$ (type A) | $P(4000),\ P(0400),\ P(0040),\ P(0004) \leq \frac{3}{32}$ | 120 | 100% |

[a]For each configuration, indicated with $m$ and $n$, type A inputs include inputs, which are equivalent to $|1^n 0^{m-n}\rangle$ up to permutation, while type B inputs are equivalent to $|n, 0, \ldots, 0\rangle$. $P(i)$ denotes the probability of obtaining the outcome $|i\rangle$. The last two columns report the number of measured states and the fraction of states satisfying the constraints, considering as successful states those compatible with the corresponding constraint within the error bars (first value) and within twice the error bars (value in parentheses). Error bars are computed with bootstrapping techniques, considering standard Poissonian uncertainties on the experimental measurement events.

which prevents the implementation of state preparation layers required for multi-photon-per-mode inputs. Additionally, in the $n = 3$, $m = 3$ scenario, we examine the input state of the form $|s\rangle = |2, 1, 0\rangle$, which does not fall under type A or type B classifications, but for which we can use the generalized constraint of Eq. (9). The derived constraints for each scenario, obtained using Eqs. (3), (8), and (9), are summarized in Table 1. The experimentally measured full-bunching probabilities for each configuration are presented through scatter plots in Figs. 2(b)–2(d), where the constraint regions are highlighted in different colors: gray cubes for type A inputs, orange surfaces for type B inputs, and green cube for the specific $|2, 1, 0\rangle$ input. In all cases error bars are associated with experimental data considering uncertainties in photon detection counts due to Poisson statistics. In Table 1, we also provide a summary of our results across different experimental configurations. For each scenario, varying both the number of modes $m$ and the input state $|s\rangle$, we list the number of recorded states, each with a different random unitary transformation $U \in SU(m)$. The table also includes the fraction of states satisfying the constraints. For both equality and inequality constraints, we consider as successful states those whose full-bunching populations are compatible with the corresponding constraint surface or volume within their

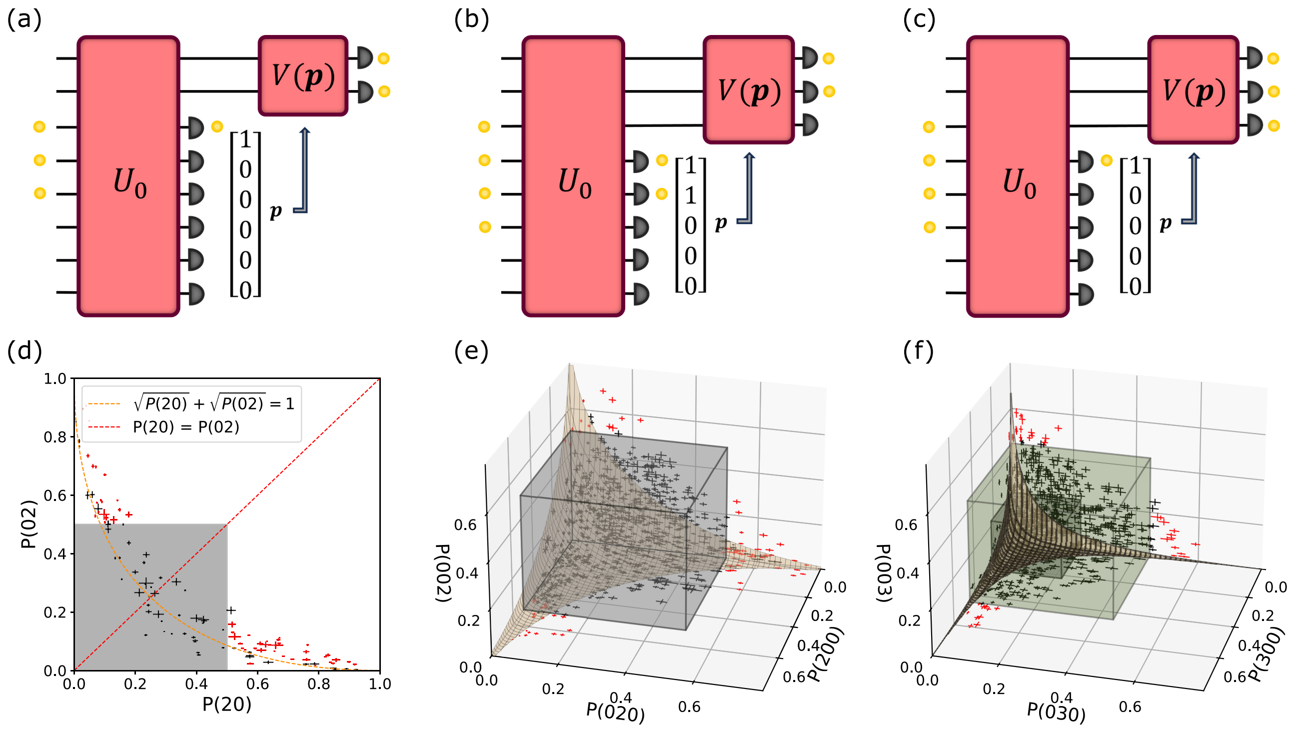


**Fig. 3.** (a)–(c) Schematics of the experimental configurations with $m = 8$ total modes and $n = 3$ (a) or $n = 4$ (b), (c) input photons, used to probe measurement-induced non-linear dynamics. The scheme we employ corresponds to an ABS implementation, where the measurement-induced adaptive evolution is emulated via post-selection. Nonlinearity is introduced by measuring $r = 1$ (a), (c) or $r = 2$ (b) photons in $k = 6$ (a) or $k = 5$ (b), (c) auxiliary modes, resulting in effective output states with $n' = n - r$ photons in $m' = m - k$ modes: ($n' = 2$, $m' = 2$) (a), ($n' = 2$, $m' = 3$) (b), and ($n' = 3$, $m' = 3$) (c). (d) 2D scatter plot of the experimentally measured bunching probabilities for the $n' = 2$, $m' = 2$ case. Full-bunching constraints under linear optics are shown as: gray square ($|1, 1\rangle$ input) and orange dashed line ($|0, 2\rangle$ input). (e) 3D scatter plot of bunching probabilities for $n' = 2$, $m' = 3$. Full-bunching constraints under linear optics are represented by: gray cube ($|110\rangle$ input) and orange surface ($|200\rangle$ input). (f) 3D scatter plot for $n' = 3$, $m' = 3$, with linear-optical boundaries given by: gray cube ($|111\rangle$), green cube ($|210\rangle$), and orange surface ($|300\rangle$). In all cases, red points indicate output states that violate all the corresponding constraints within experimental uncertainties, which are estimated from single-photon counts assuming Poisson statistics.

experimental error bars. Notably, when considering an uncertainty range of twice the experimental error bars, at least 99% of the states result compatible with the constraint boundaries, showing that full-bunching probability constraints act as an effective necessary condition for the output distribution of boson sampling experiments. We stress that, since satisfying the bounds is a necessary but not sufficient condition for linear optical evolution, these results should not be interpreted as a certification of linear optical dynamics, but rather as a verification that the necessary condition is satisfied in the probed configurations.

## 5. TESTING THE CONSTRAINTS IN NON-LINEAR DYNAMICS

We extend here our analysis of full-bunching probabilities to a regime that goes beyond standard linear optical evolution by introducing measurement-induced nonlinearities. As detailed in Section 3, in an optical implementation corresponding to an ABS protocol, a subset of the photons is measured in auxiliary modes, and the subsequent evolution of the remaining photons depends on the measurement outcome, with the whole process emulated via post-selection.

Figures 3(a)–3(c) illustrate the conceptual schemes of the employed ABS configurations. We performed experiments with $n = 3$ or $n = 4$ input photons injected into the eight-mode interferometer. In the implemented schemes, all photons evolve under an initial unitary transformation $U_0$, and a subset of $r = 1$ or $r = 2$ photons is measured in $k = 6$ or $k = 5$ auxiliary modes, leading to a measurement outcome encoded in the bit-string $\boldsymbol{p}$. The unmeasured photons then propagate through a second unitary transformation $V(\boldsymbol{p})$, which is adaptively conditioned to the outcome $\boldsymbol{p}$. This results in effective output states with $n' = 2$ or $n' = 3$ photons in $m' = 2$ or $m' = 3$ modes.

In Figs. 3(d)–3(f), we report scatter plots of the measured full-bunching probabilities for the output states obtained in the different scenarios. These distributions are compared with the theoretical boundaries imposed by linear optics for equivalent scenarios, that is, for the same number of output photons $n'$ and modes $m'$. We stress that, since the derived bounds provide necessary conditions for linear optical evolution, any violation of these bounds directly witnesses dynamics beyond linear optics. Table 2 summarizes the corresponding results, reporting the total number of reconstructed states and the fraction that violate all applicable linear-optical constraints within the experimental uncertainty. Specifically, we observe violations in 47.2% of the states for ($n' = 2$, $m' = 2$), 7.6% for ($n' = 2$, $m' = 3$), and 4.9% for ($n' = 3$, $m' = 3$). In all cases, a significant fraction of states lies beyond the boundaries defined by linear optics, providing a

**Table 2. Constraints on Full-Bunching Probabilities Tested in the Non-Linear Regime with $n'=2$ or $n'=3$ Output Photons in $m'=2$ or $m'=3$ Modes[a]**

| $n'$ | $m'$ | Equivalent Fock State | Constraint on Full-Bunching Probabilities | # States | States Violating All Constraints |
|---|---|---|---|---|---|
| 2 | 2 | $\|1,1\rangle$ (type A)<br>$\|2,0\rangle$ (type B) | $P(20),\ P(02) \le \frac{1}{2}$<br>$\sqrt{P(20)}+\sqrt{P(02)}=1$ | 108 | 47.2% |
| 2 | 3 | $\|1,1,0\rangle$ (type A)<br>$\|2,0,0\rangle$ (type B) | $P(200),\ P(020),\ P(002) \le \frac{1}{2}$<br>$\sqrt{P(200)}+\sqrt{P(020)}+\sqrt{P(002)}=1$ | 850 | 7.6% |
| 3 | 3 | $\|1,1,1\rangle$ (type A)<br>$\|2,1,0\rangle$<br>$\|3,0,0\rangle$ (type B) | $P(300),\ P(030),\ P(003) \le \frac{2}{9}$<br>$P(300),\ P(030),\ P(003) \le \frac{4}{9}$<br>$\sqrt[3]{P(300)}+\sqrt[3]{P(030)}+\sqrt[3]{P(003)}=1$ | 800 | 4.9% |

[a]For each equivalent Fock input state, the corresponding theoretical constraint under linear optical evolution is indicated. In the last two columns, we report the total number of experimentally reconstructed output states and the fraction of them that violate all the corresponding constraints within the error bars.

clear experimental signature of measurement-induced non-linear dynamics.

To further support this interpretation, we performed numerical simulations of the same ABS configurations implemented experimentally, sampling each time $\mathcal{O}(10^3)$ random unitary transformations $U_0$. The simulations predict violation fractions of 52.6%, 14.5%, and 6.7% for the cases $(n'=2, m'=2)$, $(n'=2, m'=3)$, and $(n'=3, m'=3)$, respectively. These values are in good qualitative agreement with the experimentally observed fractions. The systematically smaller violation rates observed experimentally are consistent with experimental imperfections. In particular, partial photon distinguishability is expected to reduce multi-photon interference effects and therefore suppress full-bunching probabilities, leading to a reduction in the observed violation rates. Other imperfections are expected to have a more limited impact on the observed violations. In our experiment, propagation losses inside the photonic circuit are mode-independent by construction and can be effectively modeled as a global loss channel acting after an otherwise unitary transformation. As such, they do not affect the relative output probabilities relevant for the bounds considered here. Residual mode-dependent effects, such as variations in detector efficiencies, are independently calibrated and accounted for in the data analysis.

In Supplement 1, we discuss the scalability of this witnessing approach, namely the behavior of violation rates as both the number of output photons and modes increase, providing analytical scaling arguments together with numerical simulations. Importantly, we show that the typical full-bunching probabilities for random unitaries decrease rapidly with increasing system size, leading to an exponential suppression of violation rates. As a consequence, both the identification of suitable interferometer configurations and the statistical estimation of the corresponding probabilities become increasingly demanding as the number of photons and modes grows. For this reason, the witnessing method proposed here is best suited for small- to intermediate-scale systems.

## 6. DISCUSSION

In this work, we derived and experimentally tested fundamental constraints on boson sampling output probabilities, specifically focusing on full-bunching events. These constraints highlight intrinsic limitations of linear optics in generating arbitrary output states, showing that certain output populations are inherently bounded by the nature of bosonic interference. As such, they offer new insights into the structure of boson sampling output distributions and the limitations of linear-optical transformations.

We then extended our investigation to experimental configurations that include intermediate measurements, thereby introducing effective non-linear dynamics through post-selection. In this regime, we observed a non-negligible fraction of output states that violate the full-bunching constraints derived for linear optics. This provides direct evidence that measurement-induced processes can access regions of the output space that are otherwise forbidden by purely linear evolution.

Taken together, these results show that full-bunching probabilities provide a simple and experimentally accessible witness of the boundary between linear and non-linear quantum optical behavior in small- to intermediate-scale systems, where moderate photon numbers and non-negligible collision probabilities allow for the direct observation of measurement-induced non-linear effects. In this regime, they can serve as a practical tool for benchmarking near-term photonic platforms aiming to go beyond standard linear optics.

**Funding.** European Research Council (QU-BOSS, 884676); Ministero dell'Università e della Ricerca (PE0000023-NQSTI (Spoke 4 and Spoke 7)); European Union's Horizon Europe Research and Innovation Program (EPIQUE Project (101135288)).

**Acknowledgment.** We thank an anonymous reviewer for suggesting the general bound for the full-bunching probability. Fabrication of the femtosecond laser-written integrated circuit was partially performed at PoliFAB, the micro and nano-fabrication facility of Politecnico di Milano [59]. F.C. and R.O. wish to thank the PoliFAB staff for the valuable technical support.

**Disclosures.** G. Co. and R.O. are co-founders of Ephos. The other authors declare no competing interests.

**Data availability.** Data underlying the results presented in this paper are not publicly available at this time but may be obtained from the authors upon reasonable request.

**Supplemental document.** See Supplement 1 for supporting content.

## REFERENCES

1. S. Aaronson and A. Arkhipov, "The computational complexity of linear optics," in *Proceedings of the Forty-Third Annual ACM Symposium on Theory of Computing, STOC'11 (ACM)* (2011), pp. 333–342.
2. D. J. Brod, E. F. Galvão, A. Crespi, *et al.*, "Photonic implementation of boson sampling: a review," Adv. Photonics **1**, 034001 (2019).
3. Y.-H. Deng, Y.-C. Gu, H.-L. Liu, *et al.*, "Gaussian boson sampling with pseudo-photon-number-resolving detectors and quantum computational advantage," Phys. Rev. Lett. **131**, 150601 (2023).

4. H. Wang, J. Qin, X. Ding, *et al.*, "Boson sampling with 20 input photons and a 60-mode interferometer in a $10^{14}$-dimensional hilbert space," Phys. Rev. Lett. **123**, 250503 (2019).
5. M. A. Broome, A. Fedrizzi, S. Rahimi-Keshari, *et al.*, "Photonic boson sampling in a tunable circuit," Science **339**, 794–798 (2013).
6. J. B. Spring, B. J. Metcalf, P. C. Humphreys, *et al.*, "Boson sampling on a photonic chip," Science **339**, 798–801 (2013).
7. M. Tillmann, B. Dakić, R. Heilmann, *et al.*, "Experimental boson sampling," Nat. Photonics **7**, 540–544 (2013).
8. A. Crespi, R. Osellame, R. Ramponi, *et al.*, "Integrated multimode interferometers with arbitrary designs for photonic boson sampling," Nat. Photonics **7**, 545–549 (2013).
9. J. Loredo, M. Broome, P. Hilaire, *et al.*, "Boson sampling with single-photon fock states from a bright solid-state source," Phys. Rev. Lett. **118**, 130503 (2017).
10. Y. He, X. Ding, Z.-E. Su, *et al.*, "Time-bin-encoded boson sampling with a single-photon device," Phys. Rev. Lett. **118**, 190501 (2017).
11. J. Wang, S. Paesani, R. Santagati, *et al.*, "Experimental Quantum Hamiltonian Learning," Nat. Phys. **13**, 551–555 (2017).
12. H.-S. Zhong, Y. Li, W. Li, *et al.*, "12-photon entanglement and scalable scattershot boson sampling with optimal entangled-photon pairs from parametric down-conversion," Phys. Rev. Lett. **121**, 250505 (2018).
13. N. Spagnolo, C. Vitelli, M. Bentivegna, *et al.*, "Experimental validation of photonic boson sampling," Nat. Photonics **8**, 615 –620 (2014).
14. J. Carolan, J. D. A. Meinecke, P. J. Shadbolt, *et al.*, "On the experimental verification of quantum complexity in linear optics," Nat. Photonics **8**, 621–626 (2014).
15. M. C. Tichy, K. Mayer, A. Buchleitner, *et al.*, "Stringent and efficient assessment of boson-sampling devices," Phys. Rev. Lett. **113**, 020502 (2014).
16. M. Bentivegna, N. Spagnolo, C. Vitelli, *et al.*, "Bayesian approach to boson sampling validation," Int. J. Quantum Inf. **12**, 1560028 (2014).
17. M. Walschaers, J. Kuipers, J.-D. Urbina, *et al.*, "Statistical benchmark for BosonSampling," New J. Phys. **18**, 032001 (2016).
18. I. Agresti, N. Viggianiello, F. Flamini, *et al.*, "Pattern recognition techniques for boson sampling validation," Phys. Rev. X **9**, 011013 (2019).
19. D. J. Brod, E. F. Galvão, N. Viggianiello, *et al.*, "Witnessing genuine multiphoton indistinguishability," Phys. Rev. Lett. **122**, 063602 (2019).
20. T. Giordani, D. J. Brod, C. Esposito, *et al.*, "Experimental quantification of four-photon indistinguishability," New J. Phys. **22**, 043001 (2020).
21. U. Chabaud, D. Markham, and A. Sohbi, "Quantum machine learning with adaptive linear optics," Quantum **5**, 496 (2021).
22. F. Hoch, E. Caruccio, G. Rodari, *et al.*, "Quantum machine learning with adaptive boson sampling via post-selection," Nat. Commun. **16**, 902 (2025).
23. L. Monbroussou, E. Z. Mamon, H. Thomas, *et al.*, "Towards quantum advantage with photonic state injection," arXiv (2024).
24. J. J. Moyano-Fernández and J. C. Garcia-Escartin, "Linear optics only allows every possible quantum operation for one photon or one port," Opt. Commun. **382**, 237–240 (2017).
25. P. Migdał, J. Rodríguez-Laguna, M. Oszmaniec, *et al.*, "Multiphoton states related via linear optics," Phys. Rev. A **89**, 062329 (2014).
26. J. C. Garcia-Escartin, V. Gimeno, and J. J. Moyano-Fernández, "Method to determine which quantum operations can be realized with linear optics with a constructive implementation recipe," Phys. Rev. A **100**, 022301 (2019).
27. P. V. Parellada, V. G. i Garcia, J. J. Moyano-Fernández, *et al.*, "No-go theorems for photon state transformations in quantum linear optics," Results Phys. **54**, 107108 (2023).
28. P. V. Parellada, V. G. i Garcia, J. J. Moyano-Fernández, *et al.*, "Lie algebraic invariants in quantum linear optics," arXiv (2024).
29. G. Rodari, T. Francalanci, E. Caruccio, *et al.*, "Observation of lie algebraic invariants in quantum linear optics," arXiv (2025).
30. B. Yang, H. Zhan, M. Mi, *et al.*, "Experimental observation of purity-like invariants of multi-photon states in linear optics," arXiv (2025).
31. N. Spagnolo, C. Vitelli, L. Sansoni, *et al.*, "General rules for bosonic bunching in multimode interferometers," Phys. Rev. Lett. **111**, 130503 (2013).
32. V. Shchesnovich, "Universality of generalized bunching and efficient assessment of boson sampling," Phys. Rev. Lett. **116**, 123601 (2016).
33. B. Seron, L. Novo, and N. J. Cerf, "Boson bunching is not maximized by indistinguishable particles," Nat. Photonics **17**, 702 –709 (2023).
34. A. J. Menssen, A. E. Jones, B. J. Metcalf, *et al.*, "Distinguishability and many-particle interference," Phys. Rev. Lett. **118**, 153603 (2017).
35. A. E. Jones, A. J. Menssen, H. M. Chrzanowski, *et al.*, "Multiparticle interference of pairwise distinguishable photons," Phys. Rev. Lett. **125**, 123603 (2020).
36. L. Valiant, "The complexity of computing the permanent," Theor. Comput. Sci. **8**, 189–201 (1979).
37. C. K. Hong, Z. Y. Ou, and L. Mandel, "Measurement of subpicosecond time intervals between two photons by interference," Phys. Rev. Lett. **59**, 2044–2046 (1987).
38. F. Bouchard, A. Sit, Y. Zhang, *et al.*, "Two-photon interference: the hong–ou–mandel effect," Rep. Prog. Phys. **84**, 012402 (2020).
39. S. Aaronson and T. Hance, "Generalizing and derandomizing gurvits's approximation algorithm for the permanent," arXiv (2012).
40. G. Rodari, L. Novo, R. Albiero, *et al.*, "Semi-device independent characterization of multiphoton indistinguishability," PRX Quantum **6**, 020340 (2024).
41. G. Rodari, C. Fernandes, E. Caruccio, *et al.*, "Experimental observation of counter-intuitive features of photonic bunching," arXiv (2024).
42. E. Caruccio, D. Maragnano, G. Rodari, *et al.*, "Experimental verification of threshold quantum state tomography on a fully-reconfigurable photonic integrated circuit," arXiv (2025).
43. E. Caruccio, S. Roncallo, V. Cimini, *et al.*, "Quantum analog-to-digital converter for phase estimation," arXiv (2025).
44. P. Michler, *Quantum Dots for Quantum Information Technologies* (Springer, 2017), Vol. **237**.
45. P. Senellart, G. Solomon, and A. White, "High-performance semiconductor quantum-dot single-photon sources," Nat. Nanotechnol. **12**, 1026–1039 (2017).
46. T. Heindel, J.-H. Kim, N. Gregersen, *et al.*, "Quantum dots for photonic quantum information technology," Adv. Opt. Photonics **15**, 613 –738 (2023).
47. M. Esmann, S. C. Wein, and C. Antón-Solanas, "Solid-state single-photon sources: recent advances for novel quantum materials," Adv. Funct. Mater. **34**, 2315936 (2024).
48. O. Gazzano, S. M. de Vasconcellos, C. Arnold, *et al.*, "Bright solid-state sources of indistinguishable single photons," Nat. Commun. **4**, 1425 (2013).
49. A. K. Nowak, S. L. Portalupi, V. Giesz, *et al.*, "Deterministic and electrically tunable bright single-photon source," Nat. Commun. **5**, 3240 (2014).
50. N. Somaschi, V. Giesz, L. De Santis, *et al.*, "Near-optimal single-photon sources in the solid state," Nat. Photonics **10**, 340–345 (2016).
51. H. Ollivier, I. M. de Buy Wenniger, S. Thomas, *et al.*, "Reproducibility of high-performance quantum dot single-photon sources," ACS Photonics **7**, 1050–1059 (2020).
52. G. Marshall, A. Politi, J. Matthews, *et al.*, "Laser written waveguide photonic quantum circuits," Opt. Express **17**, 12546–12554 (2009).
53. G. Corrielli, A. Crespi, and R. Osellame, "Femtosecond laser micromachining for integrated quantum photonics," Nanophotonics **10**, 3789–3812 (2021).
54. W. R. Clements, P. C. Humphreys, B. J. Metcalf, *et al.*, "Optimal design for universal multiport interferometers," Optica **3**, 1460–1465 (2016).
55. F. Flamini, L. Magrini, A. S. Rab, *et al.*, "Thermally reconfigurable quantum photonic circuits at telecom wavelength by femtosecond laser micromachining," Light Sci. Appl. **4**, e354 (2015).
56. F. Ceccarelli, S. Atzeni, A. Prencipe, *et al.*, "Thermal phase shifters for femtosecond laser written photonic integrated circuits," J. Lightwave Technol. **37**, 4275–4281 (2019).
57. F. Ceccarelli, S. Atzeni, C. Pentangelo, *et al.*, "Low power reconfigurability and reduced crosstalk in integrated photonic circuits fabricated by femtosecond laser micromachining," Laser Photonics Rev. **14**, 2000024 (2020).
58. F. Ceccarelli, J. V. Rakonjac, S. Grandi, *et al.*, "Integrated thermo-optic phase shifters for laser-written photonic circuits operating at cryogenic temperatures," J. Phys. Photonics **6**, 045023 (2024).
59. PoliFAB, https://www.polifab.polimi.it.